Asociación Argentina
de Mecánica Computacional

Mecánica Computacional Vol XXXIV, págs. 1181-1194 (artículo completo)
Sebastián Giusti, Martín Pucheta y Mario Storti (Eds.)
Córdoba, 8-11 Noviembre 2016

INTERSTITIAL PRESSURE DYNAMICS DUE TO BACTERIAL INFECTION

Ruy Freitas Reis[a], Rodrigo Weber dos Santos[a], Joventino de Oliveira Campos[a] and Marcelo Lobosco[a]

[a]*Graduate Program in Computational Modeling, Universidade Federal de Juiz de fora, Rua José Lourenço Kelmer, S/n - Martelos, Juiz de Fora - MG, 36036-330 - Brasil, ruyfreis@gmail.com, rodrigo.weber@ufjf.edu.br, marcelo.lobosco@ufjf.edu.br, http://www.ufjf.br/pgmc/*

Keywords: Computational Immunology; Edema Modelling; Porous Media; Partial Differential Equations; Finite Volume Method.

Abstract. Edema is often one of the symptoms found in infections along with skin warm to touch, shivering, aching muscles, pain, redness, swelling and so on. Edema is a consequence of interstitial fluid dynamics and their interactions with the immune system. When pathogens enter into the body, the natural consequence is an immunological reaction triggered by the production of cytokines by macrophages. This immunological response recruits other immune cells, the neutrophils, responsible for seeking and destroying the pathogens. This physiological process can be mathematically modeled by a nonlinear system of partial differential equations (PDE) based on porous media approach. In order to simplify the model, just neutrophils and pathogens (an unspecified bacteria) are considered. The equations that represent these populations are coupled with a pressure equation that is dynamically influenced by them, as well as by the lymphatic system. The pressure equation is modeled using the Starling hypothesis of fluid exchange and lymph flow. This coupling is a challenge due to the boundary conditions that are necessary to model the influence of the lymphatic system. The model is presented in its general three-dimensional form but is numerically solved in an one dimensional domain to make easier the comprehension of the results. The numerical method used to approach the solution of the PDE system is the finite volume method (FVM) with a first order upwind (FOU) scheme to ensure a stable solution of the advection term. Therefore, this study describes the mathematical and numerical tools used to model and solve the resulting PDE system.

1 INTRODUCTION

When a living body suffer an injury or when it becomes infected by bacteria or other antigen, it induces a complex cascade of nonspecific events called inflammatory response. Some of the symptoms may include swelling, redness, heat, pain and loss of function. On the other hand, these symptoms are the result of a physiological process. When a pathogen enters into the interstitial tissue, it triggers a chain of cytokines reactions that in turn increases the vascular permeability. The increase of the vascular permeability leads to leakage of fluid from the blood vessels, particularly at postcapillary venules, which results in an accumulation of fluid (edema) in the tissue (Abbas and Lichtman, 2012).

This paper presents an interstitial plasma flow equation coupled with a bacterial-neutrophil dynamics model resulting in a system of partial differential equations (PDE). The plasma flow is modeled as a single fluid in a porous medium, *i.e.*, the interstitial tissue. In addition, bacteria and neutrophil are considered mixed homogeneously in the interstitial fluid. Furthermore, bacteria and neutrophil interact as described by Pigozzo et al. (2012), which includes the bacterial proliferation and diffusion, the recruitment of neutrophils influenced by chemotaxis, and the bacterial killing by neutrophils.

The interstitial fluid pressure (IFP) is influenced by the capillary exchange and the lymphatic system (Guyton and Hall, 2006), *i.e.*, their regulatory mechanisms. The capillary exchange is modeled based on the Starling equilibrium hypothesis (Starling, 1896) and the rate of lymph flow is related to the IFP.

The resulting PDE system solution is approached using the finite volume method (FVM) in one dimensional domain (Versteeg and Malalasekra, 2007) and the stability of the numerical method is ensured using a first order upwind (FOU) scheme on the advection term (McDonald and Ambrosiano, 1984; Alves et al., 2016).

A previous work proposed an initial approach for coupling the bacterial infection dynamics with the dynamics of IFP (Reis et al., 2016), but without taking into account the influence of the lymphatic system. This paper proposes an initial model that considers the effect of the IFP on lymph flow coupled with a bacterial infection.

This paper is divided into 6 sections, starting with this introductory section, followed by a small review of immune system, the proposed mathematical model, the simulation results, and finally the conclusions and future works.

2 IMMUNOLOGY BACKGROUND

After a tissue injury or an infection, the innate immune system (IIS) develops an inflammatory response, changing the standard body dynamics. This paper aims to model the influence of the IIS on the IFP dynamics.

The spaces between cells are known as interstice and they represent about one sixth of the total volume of the body. The fluid that fills this space is called interstitial fluid. The excess of fluid in the body tissue is known as edema. It mainly occurs in the extracellular compartment, *i.e.*, the interstice. When an inflammatory response occurs, a large amount of chemical mediators, such as histamine, and cytokines induce the increase expression of endothelial cell-adhesion molecules (CAMs), which allow neutrophils (and other immune cells) pass through the endothelial walls of the blood vessels.

Neutrophils are the most abundant cells related to IIS and the major players in the body's fight against an infection, thus, they normally are the first immune cells to arrive at the infection site (Fox et al., 2010). During an infection, chemical signals attract neutrophils to the infection

site, in a movement called chemotaxis. Neutrophils then engulf the bacteria that causes the infection. Other immune cells, such as macrophages, also acts as phagocytic cells, but in this paper, neutrophils are used to represent all classes of phagocytic cells.

Neutrophils live a very short time. They leave the bone marrow programed to die about five days later. So, after the programed time, they commit suicide by a process known as apoptosis. During this time interval, they stay in blood stream waiting to be summoned (Sompayrac, 2012).

The inflammatory mediators that allowed neutrophils to enter into the tissue also lead to the vasodilation and the increase of the vascular permeability (Goldsby et al., 2002). This phenomenon is called extravasation, which may give rise to an extracellular edema (Guyton and Hall, 2006) because it also increases the diffusion through the capillary membrane to interstice. The lymphatic system is responsible for removing the interstitial fluid from the tissue, so the lymphatic system increases the lymph flow rate. Guyton and Hall (2006) estimate a lymph flow of about 120 ml/h or 2 to 3 liters per day in humans. Figure 1 shows the relation between interstitial fluid pressure and lymph flow in the leg of a dog. As can be observed, the normal lymph flow is very little at interstitial fluid pressures whose values are below the normal value of -6$mmHg$. However, it can increase more than 20-fold as pressure rises to 0 $mmHg$ ($i.e.$, the atmospheric pressure). So, as an attempt to counterpoise the increasing of plasma flow, the lymph system also increases its flows.

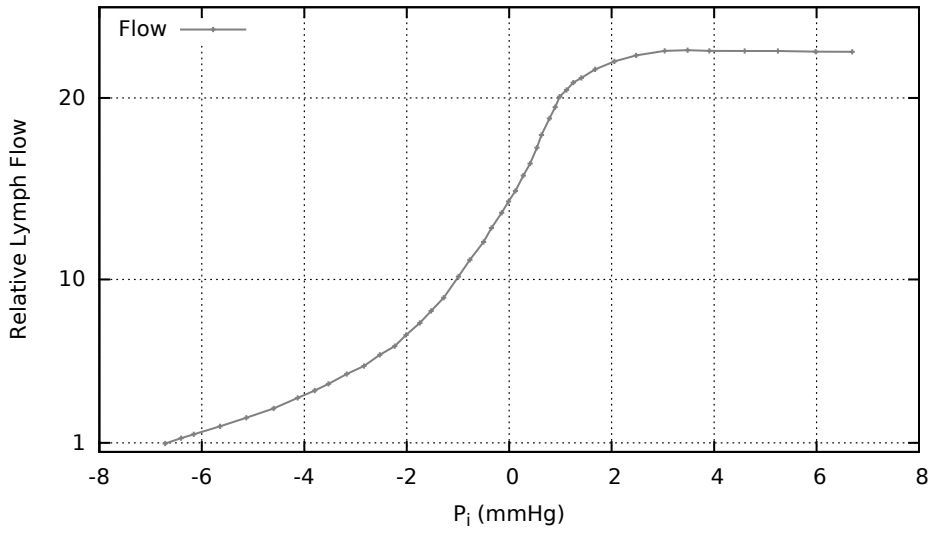

Figure 1: Relation between IFP and lymph flow in the leg of a dog. Adapted from Guyton and Hall (2006)

3 MATHEMATICAL MODEL

This section describes the mathematical model, their parameters and boundary conditions.

3.1 Interstitial Fluid Pressure

The continuum equation for a steady-state interstitial incompressible fluid is given by:

$$\nabla \cdot \vec{v}_f = q_c + q_l, \tag{1}$$

where $\vec{v}_f$ is the interstitial fluid velocity, q_c represents the capillary exchange, and q_l represents the lymphatic system.

The Darcy's equation (Eq. (2)) is used to model the interstitial fluid pressure P in a porous medium. An isotropic and homogeneous tissue is considered.

$$\vec{v}_f = -\frac{\mathbf{K}}{\mu}\nabla P, \tag{2}$$

where $\mathbf{K}$ is the medium permeability of media of the interstitial tissue, and μ is the fluid viscosity.

The capillary fluid exchange is modeled using the Starling hypothesis (Starling, 1896), according to Eq. (3).

$$q_c(P) = c_f(P_c - P - \sigma(\pi_c - \pi_i)), \tag{3}$$

where $c_f = L_p(S/V)$ is the filtering coefficient, L_p is the hydraulic permeability of the microvascular wall, and (S/V) is the vessel surface area per volume unit; P and P_c are the interstitial fluid pressure and the capillary pressure, respectively; π_c and π_i are the capillary oncotic pressure and the interstitial oncotic pressure, respectively; σ is the reflection coefficient to plasma proteins.

The plasma flux on lymph vessels is influenced by the interstitial fluid pressure. As can be observed in Figure1, the lymph flow rises until a threshold which means the limit of lymph system drainage has been achieved. The influence of the lymphatic system on the interstitial fluid dynamics is modeled by Eq. (4), which is based on the Hill equation. The parameters n, V_{max} and K_m are normally obtained from experimental data (Keener and Sneyd, 1998).

$$\iiint_V q_l(P)dV = -\left(q_0\left(1 + \frac{V_{max}(P - P_0)^n}{K_m^n + (P - P_0)^n}\right)\right), \tag{4}$$

where q_0 is the normal lymph flow.

The presence of bacteria in the interstitial tissue triggers a chain of reactions that starts with the production of cytokines, which increase the capillary permeability. Thus, the filtering coefficient is also increased, which facilitates the plasma fluid to cross from capillaries to the interstice. Eq. (5) models L_p.

$$L_p(s_b, \rho_b) = L_{p0}(1 + c_{bp}\rho_b s_b), \tag{5}$$

where L_{p0} is the hydraulic permeability of the microvascular wall in non-inflamed tissue, $s_b\rho_b$ is the bacteria concentration, and c_{bp} is the bacterial influence in the hydraulic permeability of the microvascular wall.

The interstitial fluid pressure is mathematically described by Eq. (6).

$$\begin{cases} \nabla \cdot \dfrac{\mathbf{K}}{\mu}\nabla P = -q_c(P) - q_l(P) & \text{in } \Omega \\ \alpha P + \beta \nabla P \cdot \mathbf{n} = f_p & \text{on } \partial\Omega, \end{cases} \tag{6}$$

where $\Omega \subset \mathbb{R}$, $P : \Omega \to \mathbb{R}$ and $\partial\Omega$ is the domain boundary; f_p, α and β are the parameters used to model a Robin boundary condition, which also represents lymph vessels as are shown at Table 4.

It is worthwhile to notice that the major contribution of this paper compared to our previous work (Reis et al., 2016) is the inclusion of the lymphatic system, modeled by q_l, and the new boundaries conditions which now are able to reproduce the lymphatic system.

3.2 Bacteria Dynamics

Bacteria dynamics is mathematically described by Eq. (7) using the same model of Reis et al. (2016) .

$$\begin{cases} \dfrac{\partial \phi \rho_b s_b}{\partial t} = \nabla \cdot (D_b \nabla(\rho_b s_b)) - r_b + q_b & \text{in } \Omega \times I \\ D_b \nabla s_b \cdot \mathbf{n} = f_b & \text{on } \partial\Omega \times I \\ s_b(\cdot, 0) = s_{b0} & \text{in } \Omega, \end{cases} \tag{7}$$

where $\Omega \subset \mathbb{R}$ and $I = (0, t_f] \subset \mathbb{R}^+$ is the simulation time interval, $s_b\rho_b : \Omega \times I \to \mathbb{R}^+$ is the bacterial concentration, ϕ is the medium porosity, D_b is the bacterial diffusion coefficient in the interstitial tissue, q_b is the bacterial source, and r_b is the bacterial sink.

Bacterial growing dynamics is based on the work of Pigozzo et al. (2012) and is described by Eq. (8).

$$q_b = c_b \rho_b s_b, \tag{8}$$

where c_b is the growing rate of bacteria in the interstitial tissue.

Finally, bacterial death dynamics r_b represents neutrophil-bacterial interaction, which is also based on the work of Pigozzo et al. (2012), and described by Eq. (9).

$$r_b = \lambda_{nb} \rho_n s_n \rho_b s_b, \tag{9}$$

where λ_{nb} is the bacterial death rate by neutrophil phagocytosis.

3.3 Neutrophil Dynamics

Neutrophil dynamics is mathematically described by Eq. (10), also using the same model of Reis et al. (2016).

$$\begin{cases} \dfrac{\partial \phi \rho_n s_n}{\partial t} = \nabla \cdot (D_n \nabla(\rho_n s_n) - \chi_{nb} \rho_n s_n \nabla(\rho_b s_b)) - r_n + q_n & \text{in } \Omega \times I, \\ D_n \nabla s_n \cdot \mathbf{n} = f_n & \text{on } \partial\Omega \times I \\ s_n(\cdot, 0) = s_{n0} & \text{in } \Omega, \end{cases} \tag{10}$$

where $\Omega \subset \mathbb{R}$ and $I = (0, t_f] \subset \mathbb{R}^+$ is the simulation time interval, $s_n\rho_n : \Omega \times I \to \mathbb{R}^+$ is the neutrophil concentration, D_n is the neutrophil diffusion coefficient in the interstitial tissue, χ_{nb} is the chemotaxis rate in the interstitial tissue, q_n is the neutrophil source which models neutrophil extravasation, and r_n is the neutrophil sink.

Neutrophil growing dynamics is based on extravasation, *i.e.*, their migration from the capillary to the interstice. It is represented by Eq. (11) (Pigozzo et al., 2012).

$$q_n = \gamma_n \rho_b s_b \rho_n (s_{n,max} - s_n), \tag{11}$$

where $s_{n,max}\rho_n$ is the maximum neutrophil concentration in the blood and γ_n is capillary permeability to neutrophils.

Finally, neutrophil death dynamics is influenced by neutrophil interaction with bacteria and by its natural death. It is mathematically described by Eq. (12).

$$r_n = \lambda_{bn} \rho_n s_n \rho_b s_b + \mu_n \rho_n s_n, \tag{12}$$

where λ_{bn} is the neutrophil death rate due to interaction with bacteria, *i.e.* the induced apoptosis rate, and μ_n means natural neutrophil decay.

4 NUMERICAL METHODS

In order to obtain an approximate solution of the PDE system formed by Eqs. (6), (7) and (10), the finite volume method (FVM) was used. Let $\Omega \cup \Gamma \subset \mathbb{R}$, *i.e.* an one-dimensional domain, be discretized into a set of regular nodal points defined by $\boldsymbol{S} = \{(x_i)\,; i = 0, \ldots, I_x\}$ where I_x is the number of nodal points spaced with length Δx. Furthermore, according with Figure 2, let P be any point between the domain boundary faces A and B, thus P is surrounded by a control volume. The west and east node are identified by W and E, respectively. The west and east face sides of the control volume are identified by w and e. The distance between W and P, and between P and E are identified by δ_{WP} and δ_{PE}, respectively. Moreover, the distance between w and e and P are identified by δ_{wP} and δ_{Pe}, respectively. Finally, the distance between the volume control faces is $\Delta x = \delta_{we}$. In summary, FVM is based on the evaluation of influx and outflux in a control volume around each node in the mesh.

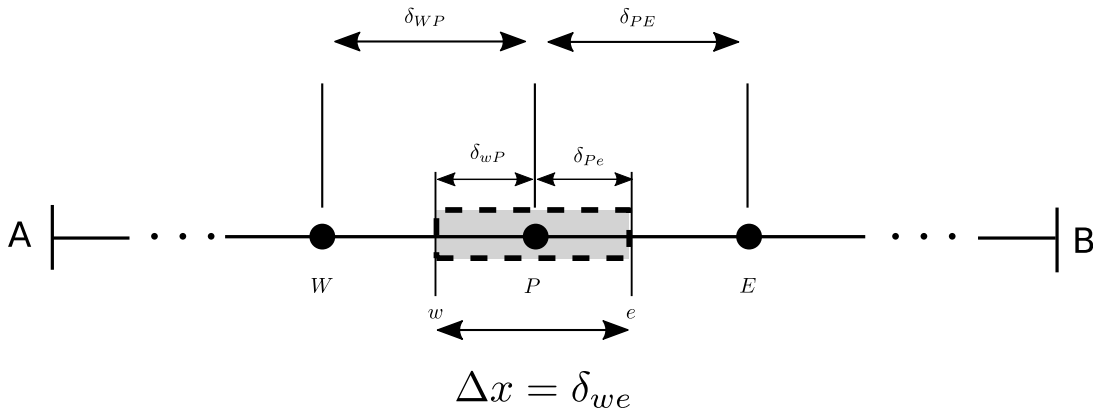

Figure 2: One-dimensional domain discretized using the finite volume method.

4.1 Interstitial Fluid Pressure

The interstitial fluid pressure equation given by Eq. (6) is discretized using the FVM, resulting in Eq. (13) which is a system composed by linear and nonlinear equations. Linear equations were solved using the Jacobi method and the nonlinear ones by a simple fixed point scheme. An error less then 10^{-8} was adopted as the convergence criteria and the error is measured using $||P_P^{k+1} - P_i^k||_\infty$.

$$\begin{cases} k_e \frac{P_E - P_P}{\Delta x} - k_w \frac{P_P - P_W}{\Delta x} + c_f(P_c - P_P - \sigma(\pi_c - \pi_i))\Delta x = 0 & \text{in } \Omega_c \\ k_e \frac{P_E - P_P}{\Delta x} - k_w \frac{P_P - P_W}{\Delta x} + q_0 \left(1 + \frac{V_{max} P_P^n}{K_m^n + P_P^n}\right) = 0 & \text{in } \Omega_l \\ k_e \frac{P_E - P_P}{\Delta x} - q_0 \left(1 + \frac{V_{max} P_P^n}{K_m^n + P_P^n}\right) + c_f(P_c - P_P - \sigma(\pi_c - \pi_i))\Delta x = 0 & \text{on } \partial\Omega_A \\ q_0 \left(1 + \frac{V_{max} P_P^n}{K_m^n + P_P^n}\right) - k_w \frac{P_P - P_W}{\Delta x} + c_f(P_c - P_P - \sigma(\pi_c - \pi_i))\Delta x = 0 & \text{on } \partial\Omega_B \end{cases} \tag{13}$$

where $\Omega_c \subset \Omega$ are the points under influence of capillary exchange; $\Omega_l \subset \Omega$ are the points under influence of the lymph system; $\partial\Omega_A$ and $\partial\Omega_B$ are the boundary of Ω at faces A and B,

respectively. Moreover, k is approached with Eq. (14).

$$\begin{cases} k_l \approx \dfrac{k_P + k_L}{2k_P k_L}, \\ k_o \approx \dfrac{k_P + k_O}{2k_P k_O}, \end{cases} \tag{14}$$

4.2 Bacteria Dynamics

Bacteria dynamics given by Eq. (7) was discretized using the FVM. The temporal derivatives were discretized using the forwarding finite difference scheme so-called Euler method. In addition to the spatial discretization, the time domain I is partitioned into N equal time intervals of length Δt, *i.e.*, $(0, t_f] = \cup_{n=0}^{N-1}[t_n, t_{n+1}]$. Thus, Eq. (7) solution approach is given by Eq. (15).

$$\begin{cases} (\rho_b s_b)_P^{n+1} = \Delta t\Big(\Phi_b((\rho_b s_b)_P^n, (\rho_b s_b)_E^n), (\rho_b s_b)_W^n) - r_b((\rho_b s_b)_P^n, (\rho_n s_n)_P^n) + q_b((\rho_b s_b)_P^n)\Big) + (\rho_b s_b)_P^n & \text{in } \Omega \\ (\rho_b s_b)_P^{n+1} = \Delta t\Big(k_l \frac{(\rho_b s_b)_E^n - (\rho_b s_b)_P^n}{\Delta x^2} - f_{tissue} - r_b((\rho_b s_b)_P^n, (\rho_n s_n)_P^n) + q_b((\rho_b s_b)_P^n)\Big) + (\rho_b s_b)_P^n & \text{on } \partial\Omega_A \\ (\rho_b s_b)_P^{n+1} = \Delta t\Big(f_{tissue} - k_o \frac{(\rho_b s_b)_P^n - (\rho_b s_b)_W^n}{\Delta x^2} - r_b((\rho_b s_b)_P^n, (\rho_n s_n)_P^n) + q_b((\rho_b s_b)_P^n)\Big) + (\rho_b s_b)_P^n & \text{on } \partial\Omega_B \end{cases} \tag{15}$$

where $\partial\Omega_A$ and $\partial\Omega_B$ are the boundary of Ω at faces A and B, respectively. Moreover, Φ_b is given by Eq. (16).

$$\Phi_b((\rho_n s_n)_P^n, (\rho_n s_n)_E^n), (\rho_n s_n)_W^n) = k_l \frac{(\rho_n s_n)_E^n - (\rho_n s_n)_P^n}{\Delta x^2} - k_o \frac{(\rho_n s_n)_P^n - (\rho_n s_n)_W^n}{\Delta x^2}, \tag{16}$$

where k is also calculated with Eq. (14).

4.3 Neutrophil Dynamics

Neutrophil dynamics given by Eq. (10) was discretized using the FVM and the temporal derivatives were discretized using the forwarding finite difference, as well. In addition, Eq. (10) needs special attention due to the chemotaxis influence. Chemotaxis term $\chi_{nb}\rho_n s_n \nabla(\rho_b s_b)$ was discretized as advection, so the use of an upwind scheme was also necessary. In this case, the First-order upwind (FOU) scheme was used. Briefly, the FOU scheme approaches the flux in the volume faces using Eq. (17).

$$(\rho_b s_b)_e = \begin{cases} (\rho_b s_b)_P & v_e > 0 \\ (\rho_b s_b)_E & v_e < 0 \end{cases} \tag{17a}$$

$$(\rho_b s_b)_w = \begin{cases} (\rho_b s_b)_W & v_w > 0 \\ (\rho_b s_b)_P & v_w < 0 \end{cases} \tag{17b}$$

Thus, it was also necessary to evaluate v_e and v_w by approaching $\nabla(\rho_b s_b)$ with a central difference scheme (Holmes, 2007).

Finally, the discrete version of Eq. (10) is given by Eq. (18).

$$\begin{cases} (\rho_n s_n)_P^{n+1} = \Delta t\Big(\Phi_n((\rho_n s_n)_P^n, (\rho_n s_n)_E^n, (\rho_n s_n)_W^n) - r_n((\rho_b s_b)_P^n, (\rho_n s_n)_P^n) + q_n((\rho_b s_b)_P^n, (\rho_n s_n)_P^n)\Big) + (\rho_n s_n)_P^n & \text{in } \Omega, \\ (\rho_n s_n)_P^{n+1} = \Delta t\Big(k_l \frac{(\rho_b s_b)_E^n - (\rho_b s_b)_P^n}{\Delta x^2} - f_{tissue} - r_n((\rho_b s_b)_P^n, (\rho_n s_n)_P^n) + q_n((\rho_b s_b)_P^n, (\rho_n s_n)_P^n))\Big) + (\rho_n s_n)_P^n & \text{on } \partial\Omega_A, \\ (\rho_n s_n)_P^{n+1} = \Delta t\Big(f_{tissue} - k_o \frac{(\rho_b s_b)_P^n - (\rho_b s_b)_W^n}{\Delta x^2} - r_n((\rho_b s_b)_P^n, (\rho_n s_n)_P^n) + q_n((\rho_b s_b)_P^n, (\rho_n s_n)_P^n))\Big) + (\rho_n s_n)_P^n & \text{on } \partial\Omega_B, \end{cases} \tag{18}$$

where $\partial\Omega_A$ and $\partial\Omega_B$ are the boundary faces A and B, respectively. Moreover, Φ_n is given by Eq. (19).

$$\Phi_n((\rho_b s_b)_P^n, (\rho_b s_b)_E^n, (\rho_b s_b)_W^n) = k_l \frac{(\rho_b s_b)_E^n - (\rho_b s_b)_P^n}{\Delta x^2} - k_o \frac{(\rho_b s_b)_P^n - (\rho_b s_b)_W^n}{\Delta x^2} - \left((\chi_{nb}\rho_n s_n)_l \frac{(\rho_b s_b)_E^n - (\rho_b s_b)_P^n}{\Delta x} - (\chi_{nb}\rho_n s_n)_o \frac{(\rho_b s_b)_P^n - (\rho_b s_b)_W^n}{\Delta x} \right) \tag{19}$$

where k is also calculated with Eq. (14).

5 RESULTS

This section presents the simulation scenario and the model results using the numerical methods described previously. The C++ programming language was chosen to implement the simulator. A numerical library, such as NAG, could be used to solve the PDEs as well. But, if an external libraries were used it would not be possible or easy to write a new parallel version to deal with complex scenarios and three-dimensional domains, as we plan to cope with in the near future. Also, few numerical libraries offer functions that are suitable to deal with this type of problem.

GNU GCC 4.9.2 was used to compile the source code using the architectural optimization flag (-march=native) in addiction to the $-O3$ flag. All simulations were performed in a SMP Linux (3.12.11-201) computer consisting of one Intel Core i7-3632QM CPU running at 2.20GHz and 6 GB of main memory.

5.1 Simulation Scenario

A summary of all parameters names, symbols, units and their respective values used in Eqs. (6), Eq. (7) and Eq. (10) are shown in Tabs. 1, 2 and 3, respectively. These values were gathered from distinct works (Phipps and Kohandel, 2011; Basser, 1992; Reis et al., 2016). μ and $\mathbf{K}$ parameters were marked with "*" because it was not found their individual values, just their relationship: $\mathbf{K}/\mu = 2.5\text{x}10^{-7} cm^2/s/mmHg$ and $L_{p0}(S/V) = 626.4(1/s/mmHg)$.

Name	**Symbol**	**Unit**	**Value**
Fluid velocity	v_f	$\frac{cm}{s}$	-
Interstitial Pressure	P	$mmHg$	-
Capillary Pressure	P_c	$mmHg$	20.0
Viscosity	μ	$\frac{g}{cms}$	*
Permeability	$\mathbf{K}$	cm^2	*
Filtering coefficient	c_f	$\frac{1}{smmHg}$	-
Hydraulic permeability	L_{p0}	$\frac{cm}{smmHg}$	$3.6\text{x}10^{-8}$
Osmotic reflection coefficient	σ_0	-	0.91
Capillary oncotic pressure	π_c	$mmHg$	20.0
Interstitial oncotic pressure	π_i	$mmHg$	10.0
Bacterial influence in hydraulic permeability	c_{bp}	$\frac{cm^3}{g}$	1.0
Normal lymph flow	q_0	$\frac{cm}{s}$	0.5
Lymph flow threshold	V_{max}	$-$	20.0
Increase flow velocity	K_m	$mmHg$	5.5
Initial pressure	P_0	$mmHg$	9.19
Exponent	n	$-$	7.0

Table 1: Model parameters values for Eq. (6).

Name	**Symbol**	**Unit**	**Value**
Porosity	ϕ	$-$	0.2
Bacteria density	ρ_b	$\frac{g}{cm^3}$	1.0
Bacteria diffusion coefficient	D_b	$\frac{cm^2}{s}$	0.0001
Bacteria reproduction rate	c_b	$\frac{1}{s}$	0.15
Phagocytosis rate	λ_{nb}	$\frac{cm^3}{sg}$	1.8

Table 2: Model parameters values for Eq. (7).

Name	Symbol	Unit	Value
Porosity	ϕ	$-$	0.2
Neutrophil density	ρ_n	$\frac{g}{cm^3}$	1.0
Neutrophil diffusion coefficient	D_n	$\frac{cm^2}{s}$	0.0001
Chemotaxis rate	χ_{nb}	$\frac{cm^5}{sg}$	0.001
Induced apoptosis rate	λ_{bn}	$\frac{cm^3}{sg}$	0.1
Capillary permeability to neutrophil	γ_n	$\frac{cm^3}{sg}$	0.1
Neutrophil source	$s_{n,max}$	$-$	0.55
Apoptosis rate	μ_n	$\frac{1}{s}$	0.2

Table 3: Model parameters values for Eq. (10).

Moreover, it is also necessary, in order to perform this simulation, to set up boundary and initial condition to Eqs.(6), (7) and (10). All their functions and values are shown at Table 4.

Variable	Initial Condition	Boundary Condition
s_n	$s_n = 0.0 \; \forall \; x \in \Omega$	$D_n \nabla s_n \cdot \vec{n} = 0 \; \forall \; x \in \partial\Omega$
s_b	$s_b = \begin{cases} 0.001 & \text{for } x \in [0.48, 0.52] \\ 0 & \text{otherwise} \end{cases}$	$D_b \nabla s_b \cdot \vec{n} = 0.0 \; \forall \; x \in \partial\Omega$
P	-	$\frac{K}{\mu} \nabla P \cdot \vec{n} = \left(q_0 \left(1 + \frac{V_{max}(P-P_0)^n}{K_m^n + (P-P_0)^n} \right) \right)$ $\forall \; x \in \partial\Omega$

Table 4: Initial and boundary conditions for the model.

According to Guyton and Hall (2006), the blood capillaries diameter are between 5 and 10 μm. On the other hand, the lymphatic capillaries diameter are about $0.2mm$, thus the caliber of lymphatics capillaries are greater than blood ones. The lymph vessels represent about 2.9% of a tissue (Rahier et al., 2011). Then it was randomly chosen points to represents lymph vessels using an uniform distribution with 2.9% of probability, otherwise it was defined as blood capillary.

5.2 Numerical Experiments

Figs. 3 and 4 show a bacterial infection controlled by netrophils. It is worth to say neutrophils and bacterias are coexisting just to highlight the pressure increase, but the neutrophil-bacteria models are able to reproduce a scenario in which the infection is eliminated (Pigozzo et al., 2012).

Moreover, Figure 3 shows that an initial infection starts at the middle of domain, more specifically at $x \in [0.48, 0.52]$ according to Table 4. Then, bacteria starts to proliferate, neutrophils leave the bloodstream and went out to the interstitial tissue. As bacteria spread out, neutrophils also follow them due to extravasation and chemotaxis. Finally, infection dynamics happens much faster than usual just to demonstrate quickly the pressure dynamics, which are the main

goal of this paper. It is possible to slow down the bacteria and neutrophil proliferation in order to reproduce their real dynamics.

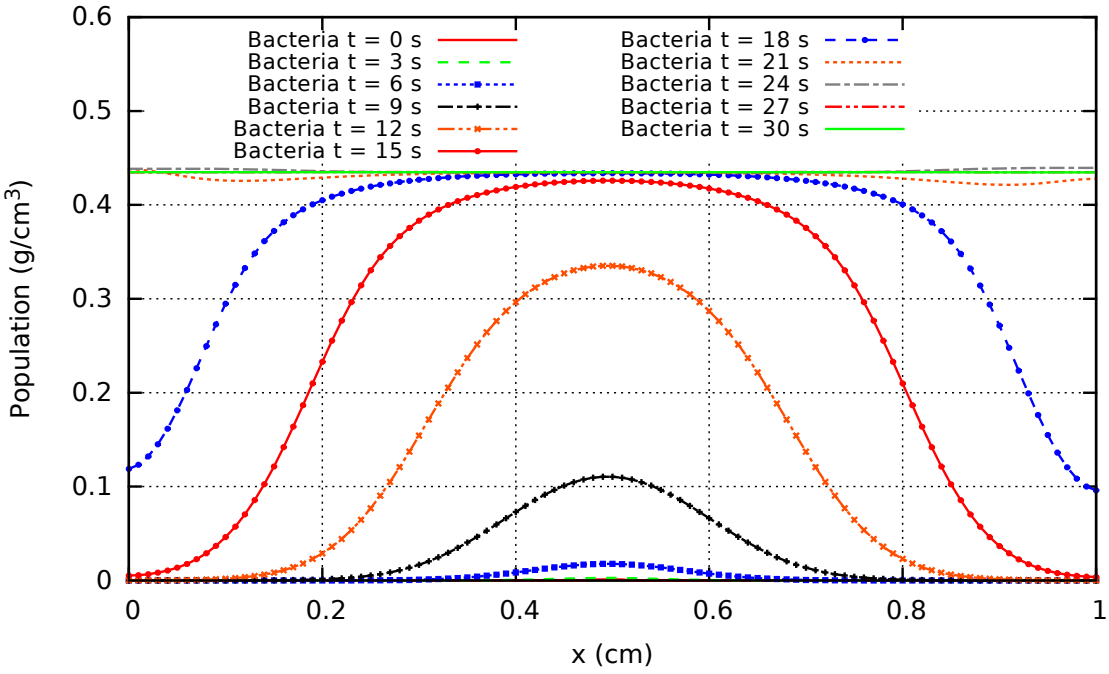

Figure 3: Bacteria dynamics.

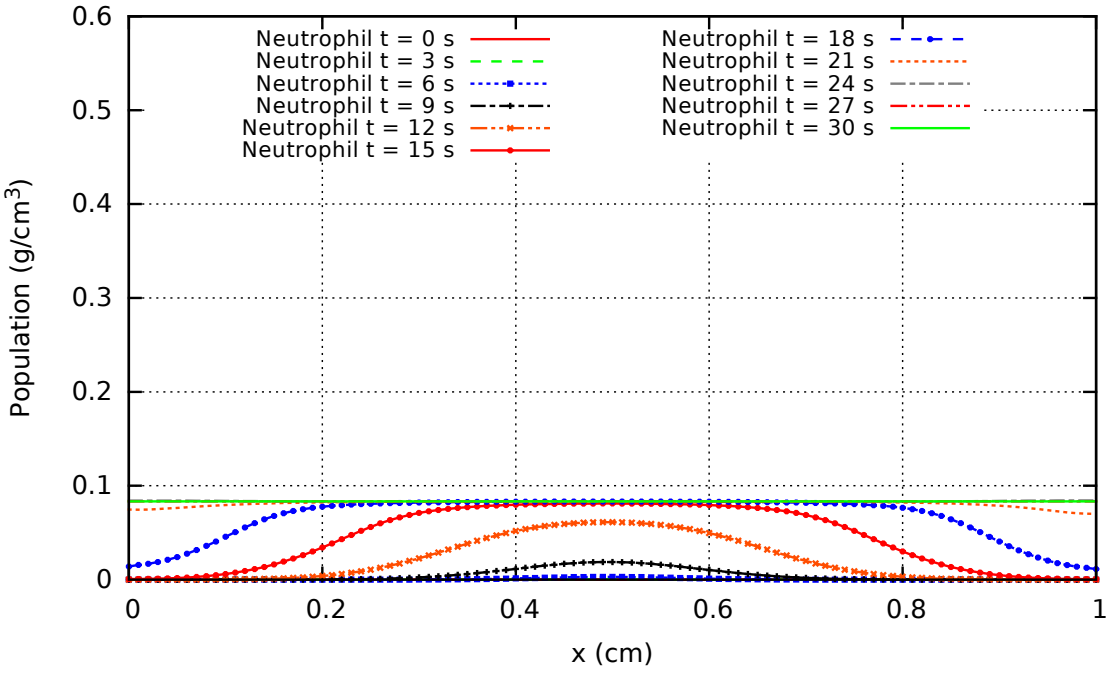

Figure 4: Neutrophil dynamics.

In addition, Figure 5 shows the IFP alteration due to the ongoing infection. At first, IFP has no alterations, but as the infection proliferates a small peak appears at $t = 6s$. It starts

to rise and spread out the domain culminating in almost a plane with just 3 points (they are also marked with a small triangle on the graphic bottom, at $x \in \{0.0, 0.4, 1.0\}$) holding the solution below. These points represent the lymphatic system influence in the IFP, according to Eq. (4). Furthermore, the lymphatics on contour are treated as boundary conditions. This pressure increase along with an uncontrolled inflammation reaction due to an infection may give rise to an extracellular edema.

On the other hand, Figure 6 shows the relationship between IFP and the relative lymph flow taken from simulation results at $x = 0.40\ cm$. These numerical results are also an attempt to validate the mathematical model considered here. Comparing them with the experimental data founded in Guyton and Hall (2006), it is possible to notice that the pressure curve at Figure 6 is qualitatively similar in its shape and range of values with the experimental data shown in Figure 1.

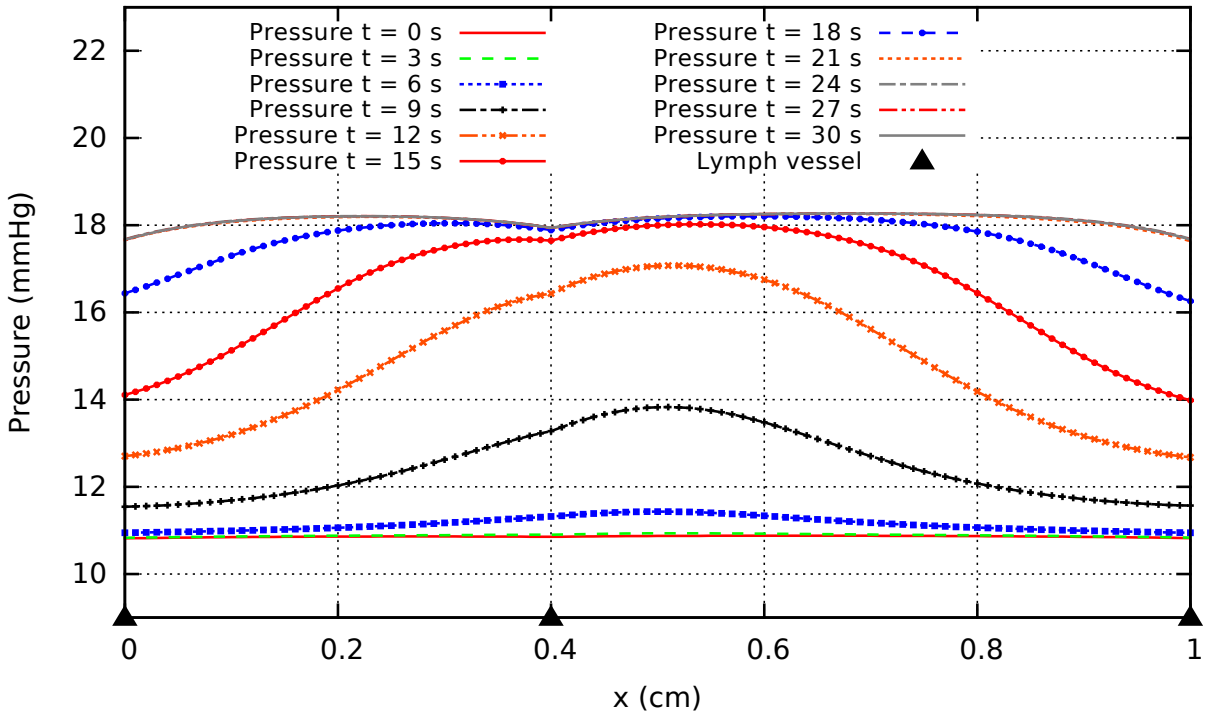

Figure 5: Pressure dynamics over the domain.

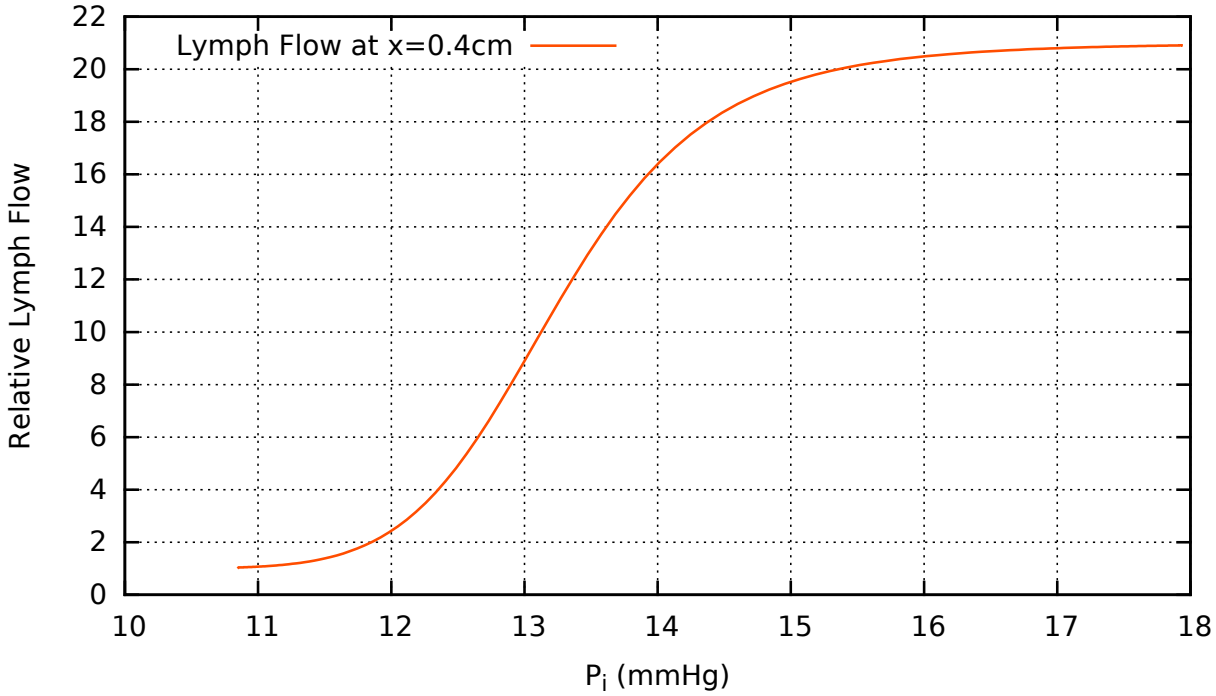

Figure 6: *In silico* results for the relationship between the IFP and the lymph flow at $x = 0.40\ cm$.

6 CONCLUSIONS AND FUTURE WORK

This paper aimed to model the influence of a pathogen in the interstitial fluid dynamics. Neutrophils were chosen to represent the innate immune system cells which were summoned to control an unspecified bacterial infection. As a result, the vascular permeability increases along with the neutrophil extravasation, thus it changes the interstitial fluid pressure dynamics which, in some cases, may lead to an extracellular edema. So, this paper has presented a model to describe all this interaction using PDEs based on a previous work (Reis et al., 2016), but now including the lymph system influence as well. Despite of some simplifications and limitations of the proposed model, the results were able to reproduce some key aspects related to an initial edema formation.

As a future work, it is planed to analyze the influence of the IFP increase in the immune system cells, more specifically if the pressure gradient may influence them.

REFERENCES

Abbas A. and Lichtman A. *Basic Immunology Updated Edition: Functions and Disorders of the Immune System*. Elsevier Health Sciences, 2012.

Alves J., de Queiroz R., and dos Santos R. Simulation of cardiac perfusion by contrast in the myocardium using a formulation of flow in porous media. *Journal of Computational and Applied Mathematics*, 295:13 – 24, 2016. ISSN 0377-0427. doi:http://dx.doi.org/10.1016/j.cam.2015.04.008. VIII Pan-American Workshop in Applied and Computational Mathematics.

Basser P.J. Interstitial pressure, volume, and flow during infusion into brain tissue. *Microvascular research*, 44(2):143–165, 1992.

Fox S., Leitch A.E., Duffin R., Haslett C., and Rossi A.G. Neutrophil apoptosis: relevance to

the innate immune response and inflammatory disease. *Journal of innate immunity*, 2(3):216–227, 2010.

Goldsby R.A., Kindt T.J., Kuby J., and Osborne B.A. *Immunology, Fifth Edition*. W. H. Freeman, 5th edition, 2002. ISBN 0716749475,9780716749479.

Guyton A. and Hall J. *Textbook of Medical Physiology*. Guyton Physiology Series. Elsevier Saunders, 2006. ISBN 9780808923176.

Holmes M.H. *Introduction to Numerical Methods in Differential Equations*. Texts in Applied Mathematics 52. Springer-Verlag New York, 1 edition, 2007. ISBN 978-0-387-30891-3.

Keener J.P. and Sneyd J. *Mathematical physiology*, volume 8. Springer, 1998.

McDonald B.E. and Ambrosiano J. High-order upwind flux correction methods for hyperbolic conservation laws. *Journal of Computational Physics*, 56(3):448–460, 1984.

Phipps C. and Kohandel M. Mathematical model of the effect of interstitial fluid pressure on angiogenic behavior in solid tumors. *Computational and mathematical methods in medicine*, 2011, 2011.

Pigozzo A.B., Macedo G.C., Weber dos Santos R., and Lobosco M. Computational modeling of microabscess formation. *Computational and mathematical methods in medicine*, 2012, 2012. doi:http://dx.doi.org/10.1155/2012/736394.

Rahier J.F., De Beauce S., Dubuquoy L., Erdual E., Colombel J.F., Jouret-Mourin A., Geboes K., and Desreumaux P. Increased lymphatic vessel density and lymphangiogenesis in inflammatory bowel disease. *Alimentary pharmacology & therapeutics*, 34(5):533–543, 2011.

Reis R.F., dos Santos R.W., and Lobosco M. *Bioinformatics and Biomedical Engineering: 4th International Conference, IWBBIO 2016, Granada, Spain, April 20-22, 2016, Proceedings*, chapter A Plasma Flow Model in the Interstitial Tissue Due to Bacterial Infection, pages 335–345. Springer International Publishing, Cham, 2016. ISBN 978-3-319-31744-1. doi: 10.1007/978-3-319-31744-1_30.

Sompayrac L. *How the Immune System Works*. Wiley-Blackwell, 2012.

Starling E.H. On the absorption of fluids from the connective tissue spaces. *The Journal of physiology*, 19(4):312–326, 1896.

Versteeg H. and Malalasekra W. *An Introduction to Computational Fluid Dynamics: The Finite Volume Method*. Prentice Hall, 2 edition, 2007. ISBN 978-0131274983.